scientific reports

Check for updates

OPEN

Titanium dioxide nanoparticles augment Ciprofloxacin activity via Inhibition of biofilm formation for multidrug resistance bacteria in-vitro and insilco prediction study

Mazin A. A. Najm[1], Hussein A. Shakir[2], Sabah T. Hasen[2], Kareem H. Jawad[2], Buthenia A. Hasoon[3], Majid S. Jabir[3]✉, Ali A. Issa[3], Salim Albukhaty[4]✉, Mansour K. Gatasheh[5]✉ & Mohammad H. Molla[6]

The increasing of multi-drug among pathogenic microbes is rendering antibiotics ineffective. Consequently, efforts are now concentrated on addressing this challenge through developing novel antibiotics and enhancing existing ones. This study combined ciprofloxacin (CIP) with titanium dioxide nanoparticles (TiO_2NPs). We characterized the prepared nanoparticles (NPs) using several methods, including UV-Vis spectra, XRD, FESEM, TEM, and FTIR. The well diffusion agar was used to study the antibacterial activity of ciprofloxacin (CIP) alone and combined with titanium dioxide nanoparticles CIP@TiO_2NPs. CIP@TiO_2NPs showed higher antibacterial activity against *Klebsiella pneumoniae* (*K. pneumoniae*) and *Streptococcus mutans S.mutans*. The CIP@TiO_2NPs showed remarkable inhibitory properties compared to CIP alone and TiO_2NP alone, with its inhibition zone 28.50 ± 0.20 and 17.50 ± 0.10 in *K.pneumoniae* and *S.mutans*, respectively. Insilico study was done on bacterial strains to describe the effective binding behavior towards the ciprofloxacin@TiO_2 adsorption system. The best conformers, from 50 conformational adsorption systems, were analyzed with a significant favorable inhibition with binding energy values of -9.61 kcal/mol and – 9.40 kcal/mol with *K.pneumoniae* and *S. mutans*, respectively. The interaction between CIP@TiO_2NPs nanoparticles and *Klebsiella pneumonia* (ID: 8JGW) was studied using 50 conformations. The results showed binding energies up to -9.61 kcal/mol, indicating high interaction efficacy. Compared to TiO_2NPs and CIP alone, CIP@TiO_2NPs displayed the highest antibacterial and anti-biofilm properties against pathogenic bacteria. CIP@TiO_2NPs have demonstrated promising results, suggesting that they may prove to be a dependable treatment for *K. pneumoniae* and *S.mutans* in the future and a possible agent for reducing bacterial biofilm during bacterial infections.

Keywords Ciprofloxacin, TiO_2 NPs, Antibacterial, MDR, Biofilm Inhibition, Insilico study

The fabrication and use of nanoparticles in biomedicine have led to breakthroughs in the characterization and modulation of intrinsic features, such as surface plasmon resonance and electrical, optical, and physicochemical properties, resulting in altered attributes[1]. Over the past 15 years, researchers have extensively studied nanoparticle characteristics for their biomedical applications[2]. This increasing interest stems from the fact that metalloids, organic/inorganic complexes, and metallic nanoparticles such as zinc and silver can be incorporated into cells via several different pathways due to their nanoscale size[3–6]. Furthermore, the physiochemical parameters of nanoparticles can significantly influence their behavior and change over time[7–10]. As a result, nanoparticles' biomedical applications offer biocompatibility, specific target recognition, and functionalization capabilities,

[1]Department of Pharmacy, Mazaya University College, Thi-Qar, Iraq. [2]Laser & Optoelectronics Engineering Department, University of Technology, Baghdad, Iraq. [3]Department of Applied Sciences, University of Technology, Baghdad, Iraq. [4]Al-Manarah College for Medical Sciences, Maysan, Iraq. [5]Department of Biochemistry, College of Science, King Saud University, P.O. Box-2455, Riyadh 11451, Saudi Arabia. [6]Rubenstein School of Environment and Natural Resources, University of Vermont, Burlington, VT 05405, USA. ✉email: 100131@uotechnology.edu.iq; albukhaty.salim@uomanar.edu.iq; albukhaty.salim@uomisan.edu.iq; mgatasheh@ksu.edu.sa

making them ideal carriers for drug delivery[11,12]. Building on this foundation, silver nanomaterials have been extensively researched for their antibacterial activity. Silver has been utilized for thousands of years in various applications, including food preservation, water sanitization, and wound healing[13,14]. However, the emergence of microbial resistance poses an important test to the effectiveness of most antibiotics globally[15,16]. In this context, bacterial antibiotic resistance employs varied mechanisms, including decreased absorption and increased efflux of drugs out of the bacterial cell wall. These mechanisms collectively diminish drug content within the cell, inhibiting microbial cytotoxicity, facilitating enzymatic modification, and reducing or inhibiting metabolic activity[17,18]. Consequently, there has been a heightened interest in nanotechnology due to its remarkable benefits in the therapeutic field[19,20]. Among the widely used nanomaterials for their anti-bacterial action are Au, Ag, P, Zn, Cu, and TiO_2[14,21].

In light of these developments, the mechanisms by which nanomaterials exhibit antibacterial properties can be understood through two key details: (a) the release of metals from the surface of NPs contributes to the toxicity of metal ions to cells, and (b) the increased generation of reactive oxygen species (ROS) on nanomaterials induces oxidative stress within microbial cells, leading to cell death[22–25]. Notably, when combined with nanoparticles, antibiotics demonstrate enhanced antibacterial properties against various microbes, which may amplify cell penetrability or compromise the cell membrane[26]. For instance, researchers have effectively synthesized citrate-layered Ag-NPs using vancomycin and examined their anti-microbial action in contradiction of *E. coli* and *S. aureus*, revealing significant improvements in antibacterial activity compared to vancomycin alone, thus demonstrating a synergistic result among the drug and Ag-NPs[27].

Transitioning to another critical aspect, ciprofloxacin (CIP), a second-generation quinolone and fluoroquinolone, is unique of the most usually used antibiotics due to its broad microbial inhibitory range against pathogens accountable for organ infections, including respiratory, urinary tract, soft tissue, intestinal, and skin infections, as well as sexually transmitted infections[28]. CIP is effective against numerous microbes accountable for community-acquired pneumonia, including *E. coli*, *H. influenzae*, and *K. pneumoniae*. Despite its widespread use, resistance to CIP has emerged in certain strains, such as *S. pyogenes* and *K. pneumoniae*[29,30]. Furthermore, while ecological risk assessments of antibiotic adsorption on TiO_2 nanoparticles have been limited, studies have described the adsorption of penicillin and ciprofloxacin on TiO_2 NPs[31–33]. Another investigation into the photocatalytic properties of TiO_2 NPs indicates the adsorption of CIP on their surfaces[34]. Given this background, the current study focuses on synthesizing titanium dioxide nanoparticles (TiO_2NPs) conjugated with ciprofloxacin (CIP) through laser ablation and evaluating their effects on antibacterial activity and biofilm formation. This investigation aims to address the pressing issue of microbial resistance, which poses an important challenge to the efficiency of antibiotics globally. Additionally, we aim to establish rigorous standards for studying the bactericidal effects of CIP@TiO_2NPs in terms of attachment dynamism and bonding distances with target pathogens through in silico analysis.

Materials and methods

Chemicals

Titanium target (Ti), and dimethyl sulfoxide (DMSO) were obtained from (Merck. Co. Germany). Nutrient agar powder, Molar Hinton agar (M.H.A), Crystal Violet (C.V. stain), Distilled Water (D.W), Ciprofloxacin antibiotic, Acridine Orange/Ethidium Bromide (AO/EtBr double stain) were obtained by (Sigma-Aldrich).

Preparation of TiO_2NPs and CIP@TiO_2NPs

Initially, titanium dioxide nanoparticles were synthesized using a throbbed laser ablation method. A Ti_2 target (10 × 10) mm two mm thick was placed at the base of a cup full of 5 ml of distal water (D.W). Next, the surface of the titanium dioxide substrate was shown to be a 1064 nm Q-switched (Nd-YAG laser) Coherent, Inc/ USA. This laser emits pulses with an energy of (500 mJ at 30 min, 9NS, 300 pulses, and rate repetition 2 Hz). The next stage is to prepare CIP@TiO_2NPs by addition of 0.001 mg of antibiotic to 100 mL of TiO_2NPs prepared with the use of Nd: YAG laser under similar conditions to produce TiO_2NPs, with stirring under sonication in instruction to increase the interface among the antibiotic and the TiO_2NPs. When the color of the solution was different from off-white (milky) to light brown, successful CIP@TiO_2NPs was achieved. Prepared with some change[35,36]. As in Fig. 1.

Characterization

The characterization of the synthesized titanium dioxide nanoparticles (TiO_2NPs) and their conjugate with ciprofloxacin (CIP) was performed using several analytical techniques:

UV–Vis spectroscopy

A Shimadzu UV-Vis spectrophotometer was used to evaluate the colloidal nanoparticles' absorption spectra in the 200–800 nm wavelength range. This analysis helps determine the optical possessions of the TiO_2NPs and their interaction with CIP[37].

Fourier transform infrared spectroscopy (FT-IR)

The chemical composition and functional groups of the CIP@TiO_2NPs were studied using FT-IR spectroscopy (B.M.S, Madrid, Spain). This method makes it possible to identify specific bonds and functional groups in the nanoparticles[38].

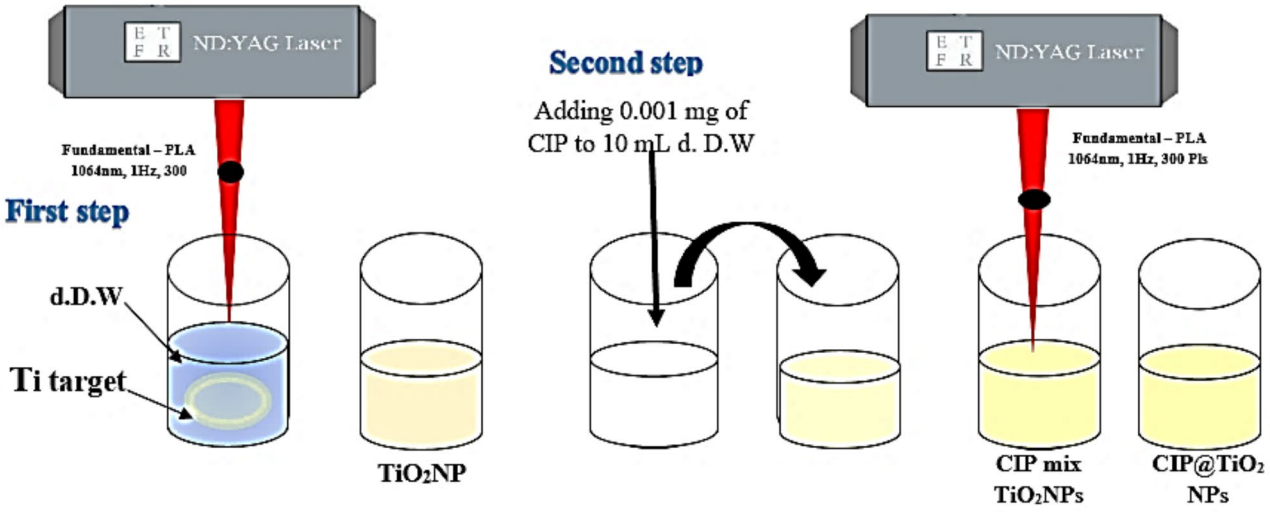

Fig. 1. Steps of preparation of TiO_2NPs and CIP@TiO_2NPs.

Scanning Electron microscopy (SEM)
The morphology and surface characteristics of the nano-composite were examined using SEM. This technique provides detailed images of the particle shape and size, contributing to the understanding of their structural properties[39].

Transmission Electron microscopy (TEM)
TEM micrographs were captured using a JEM 1010-JEOL microscope. This technique offers insights into the size and distribution of the nanoparticles at a higher resolution compared to SEM[40].

Images examination
The size of the nanoparticles was determined using Image-J software, which allows for accurate measurement of particle dimensions from the TEM images[41].

X-ray diffraction (XRD)
The crystalline structure of the TiO_2NPs and CIP@TiO_2NPs was investigated using XRD analysis with a Shimadzu XRD-6000 tool, employing a Cu-Kα radiation source. The diffraction patterns were analyzed within specific angular ranges (2θ), providing information on the crystallinity and phase composition of the nanoparticles[42].

In Silico methodology

The designed adsorption system of ciprofloxacin with TiO2 nanoparticles was generated by Materials Studio software[43], as displayed in Fig. 2. The system was prepared for molecular docking (MD) simulation as shown in Fig. 1. MD study was performed with Autodock 4.2 software[44]. Exposed Babel software was used to change the ligand's file format to PDBQT[45]. A specific protein was chosen to investigate the nanoparticle compound's bioactive characteristics. Two protein targets (K. pneumoniae ID: 8JGW and S. mutans ID: 3IHK) were utilized through the Protein Data Bank PDB (www.rcsb.org)[46]. The removal of water molecules and hetatoms, among other protein pretreatments, was regulated using the Biovia Discovery Studio software (http://www.accelrys.com). The process starts when polar hydrogens are added to the protein, Kollman charges are added, and Gasteiger charges are assigned. The protein's active site of *K. pneumoniae* (102 × 68 × 82 Å3) was intended to be covered by the grid box, and the number of user-specified grid centers of X= -21.276, Y= -30.005, and Z= -3.675. The other setting parameters of S. mutans were recorded with dimensions 74 × 48 × 92 Å3 with specified grid centers X = 18.056, Y = 15.545, and Z = 4.253. Fifty conformations/poses were found by fine-tuning docking parameters with genetic algorithms. Then, using ligand-receptor non-covalent interactions (NCIs) to demonstrate the lowest binding free energy, the best conformer was chosen.

Assessment of minimum inhibitory concentrations (MIC)

The MIC of CIP, TiO_2NPs, and CIP@TiO_2NPs against *S. mutans and K. pneumoniae* was evaluated by a micro-dilution test. Stock solutions were prepared, test micro-liter plates were set up, and the MIC was determined as the lowest concentration that inhibited visible bacterial development after 24 h[47].

Anti-bioflim test

The anti-biofilm test by well diffusion method. The anti-bacterial activities of the TiO_2NPs, CIP, and CIP@ TiO_2NPs were evaluated against two types of bacteria (*S. mutans* UA159 and *K. pneumoniae* ATCC 10031), Plates were covered with 0.5 ml quantities of the activated bacteria (1.5 × 106 CFU/mL − 1). Agar plates were coated with 80 µl of the tested agents (CIP, TiO2NPs, and CIP@TiO2NPs at a concentration of 25 µgml-1) and

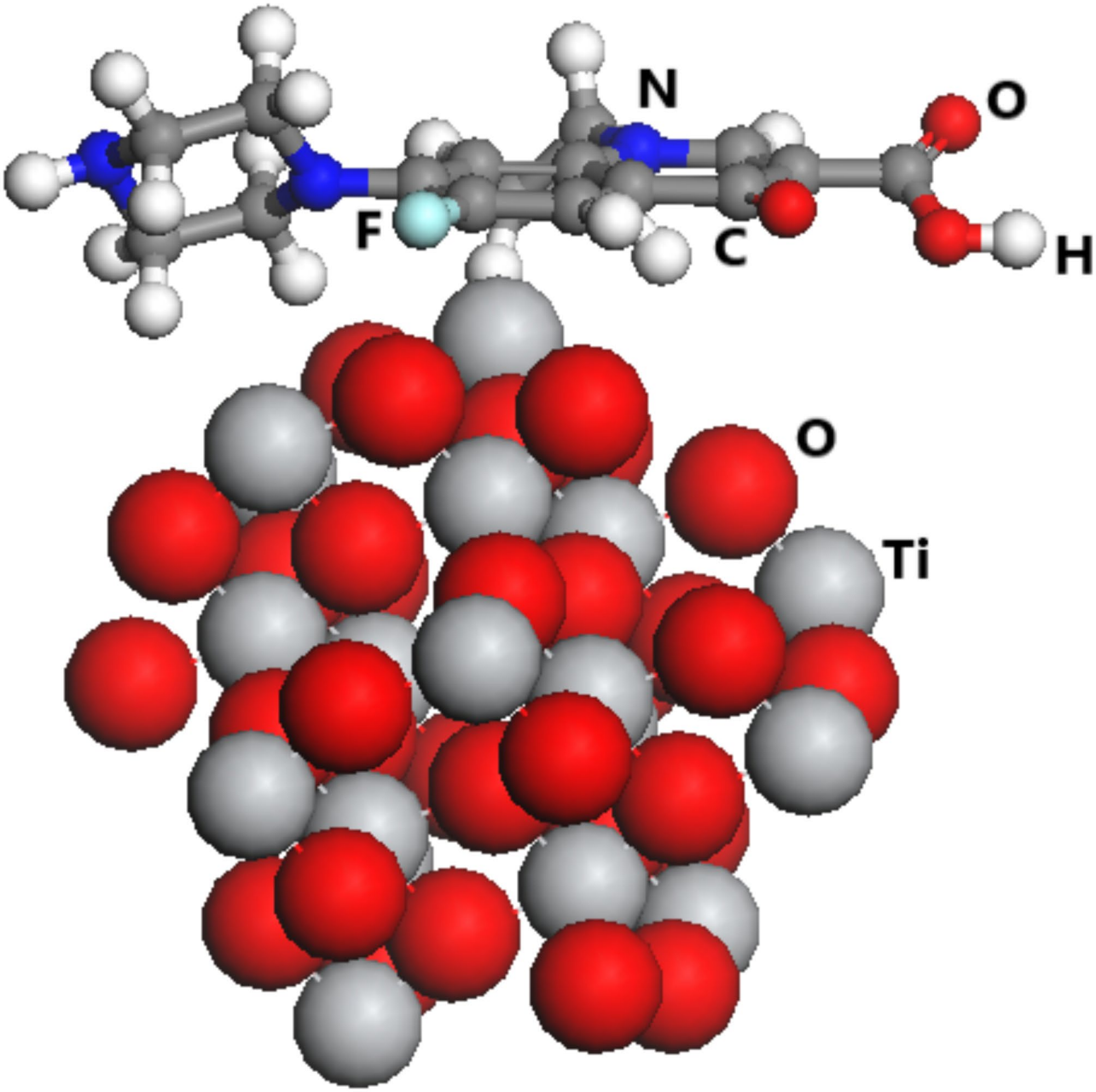

Fig. 2. The designed structure of CIP@TiO_2 NPs.

incubated at 37 °C. After 24 h. incubation, the inhibition zone was assessed, conferring to the zone of inhibition about the well. To perform the anti-biofilm test using C.V. stain, bacterial strains with concentrations of (1 * I0 ^{6} CFU/ mL^{-1}) were cultivated in 96-well plates and treated for 24 h with TiO_2NPs, CIP, and CIP@TiO2NPs. PBS wiped out the test sample. Next, bacteria at a 0.1% concentration were stained with C.V. and twice washed with DW. After adding 0.2 mL of 95% ethanol to the C.V. stained wells and shaking them for two hours, the biofilm growth was measured. A 595 nm calculation of optical density was made[48]. AO/EtBr double stain is used to study life and die bacterial strains. All experiments were approved in triplicate.

Statistical study

ANOVA and an unpaired t-test were used to statistically evaluate the collected data using GraphPad Prism[49,50]. The mean ± SD of the values was displayed[51,52].

Results and discussion

The combination of TiO_2NPs) with CIP was employed to improve the effectiveness of the antibiotic against the pathogen, resulting in a potent nano-antibiotic. The transition in color from off-white (milky) to light brown, as shown in Fig. 3, helped as a notable indicator of the compelling mixture of TiO_2NPs with CIP[53]. The

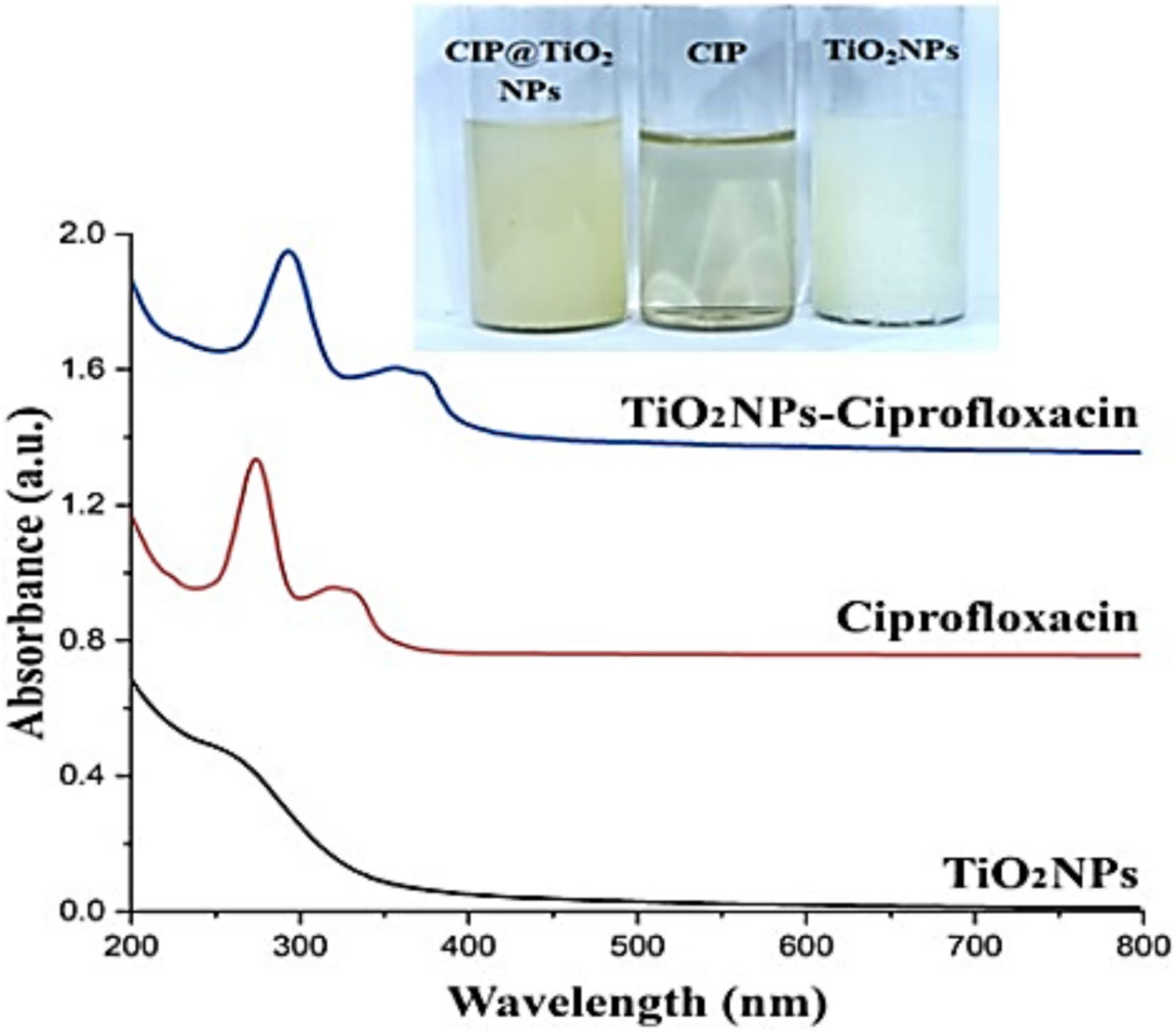

Fig. 3. UV–Vis of TiO2NPs, CIP, CIP@TiO_2NPs.

mixture did not appear to affect the essential pharmacophore groups within the structure-action relationship of CIP particles. These groups encompass the fluoro group, central for compulsory to bacterial DNA gyrase; the piperazinyl group, which moderates the drug's properties and pays to its wanted pharmaco-kinetics; and the carbonyl and carboxyl groups, recognized for their necessary to microbial gyrase. CIP particles, measured by their unique nonflat, wedge-shaped structure, unlike other fluoroquinolones, have shown meaningfully enhanced antibacterial efficiency[54]. Additionally, theoretical studies and parallel antiseptic action tests have exposed the better therapeutic properties of the CIP@TiO_2NPs mixture than of CIP alone. The CIP@TiO_2NPs were also ready as a potent, novel nano-antibiofilm agent with the utmost anti-bacterial result through laser ablation.

Figure 3 shows the absorbance of TiO_2NPs in combination with Ciprofloxacin; a UV-Vis spectrum studied the optical possessions within the spectral series of 200–800 nm. The peak at 255 nm distinguishing TiO_2NPs; as for CIP@TiO_2NPs, the distinguishing SPR peak seemed at 300 nm; the upsurge was due to the color variation, the nearby chemical setting, and the size rise of NPs as of the adsorption layer, consequently on behalf of a significant shift to the visible range subsequent the adding of CIP, i.e., by 255 to 300 nm, the absorption peak of CIP alone was experiential at 270 nm, as got formerly[55].

XRD designs for TiO_2 NPs are ready through the PLAL method by an Nd: YAG laser at 1064 nm. The XRD designs display peaks placed at $2\theta = 25.0^{o}$, 38.283^{o}, 5325^{o}, and 63.9^{o} which agree planes to (101), (210), (200), and (105) planes; these results reveal the face-centered cubic (FCC) of TiO_2 NPs rendering to known design (JCPDS card no. 21-1272), as in Fig. 4 (Left panel), these results are reliable by previous investigation. Furthermore, CIP@TIO2NPs showed similar peaks at angles 28.55, 38.21, 40.11, 48.21, and 62. 13 representing the (110),

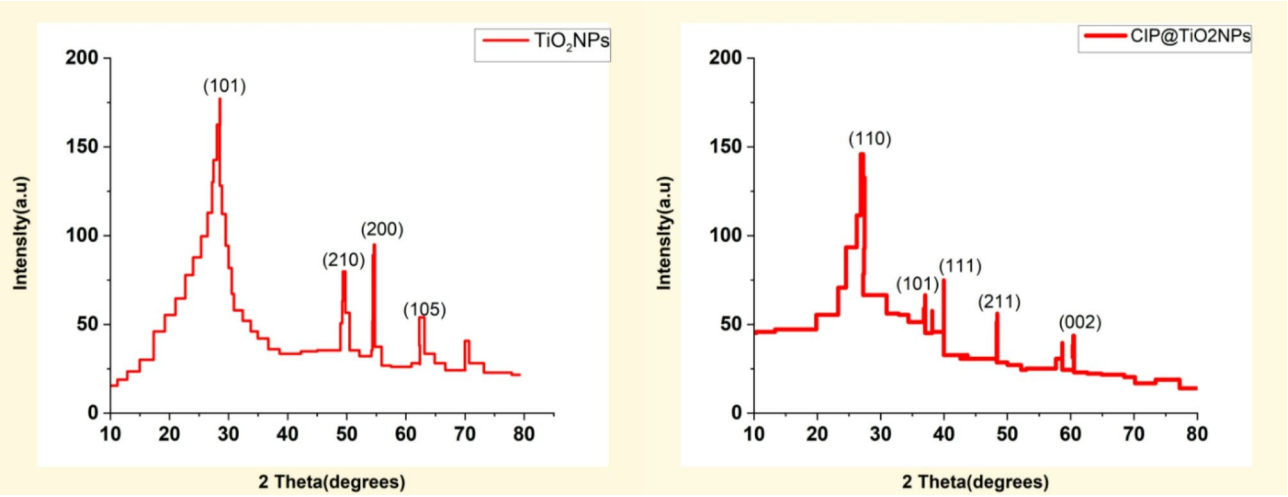

Fig. 4. XRD of TiO_2NPs (Left panel), and CIP@TiO_2NPs (Right panel).

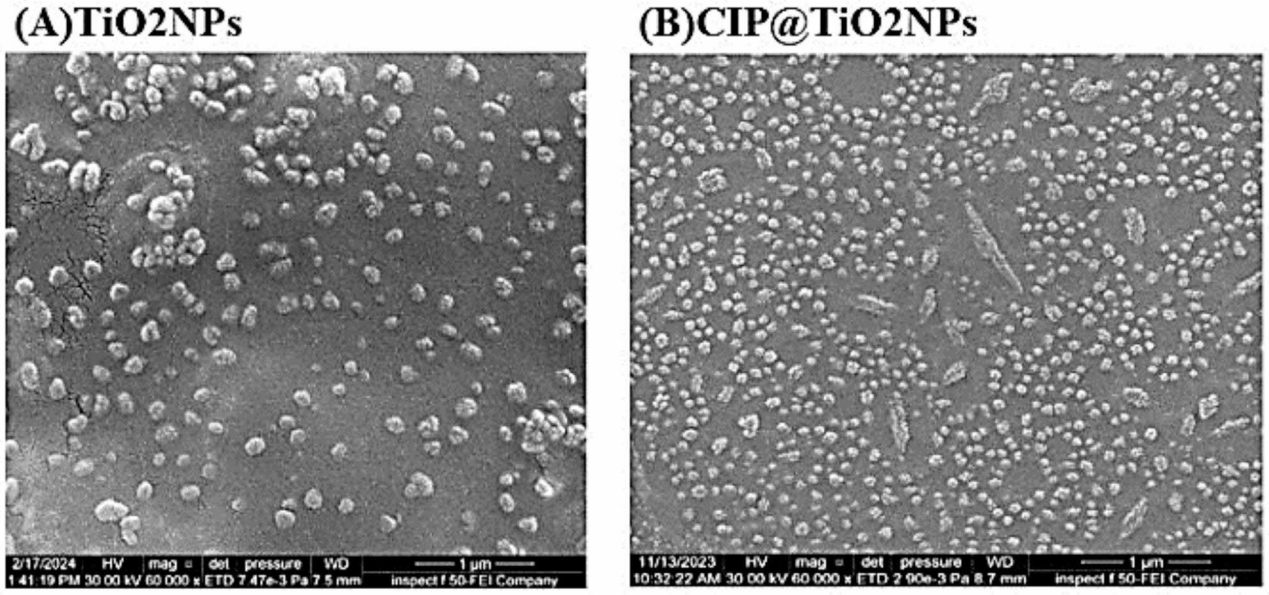

Fig. 5. FE-SEM image for (**A**) TiO_2NPs, (**B**) CIP@TiO_2NPs.

(101), (111), (211), and (002) planes, respectively, as shown in Fig. 4 (Right panel). These consequences are arranged in previous studies. The XRD data designated the regular size of TiO_2 NPs using Scherer's equation[56].

The size and shape of TiO_2NPs and (CIP@TiO_2NPs) prepared by the PLAL technique depend significantly on the parameters of the pulsed laser used as the ablation source, especially the fluence of the pulsed laser. The NPs were identified using FE-SEM and TEM. TiO_2NPs' morphological traits details, which include smooth surfaces and spherical forms with specific accumulation and aggregation of nanoparticles, were revealed by FE-SEM. The average volume ranges from 5 to 40 nm, with a particle size of approximately 17 nm, as indicated in Fig. 5A; when the conjugation between CIP and TiO_2 nanoparticles (CIP@TiO_2NPs) was examined, an increase in the number of NPs appeared, as the average size ranged between 10 and 50 nm and the average crystalline size was assessed to be about 27 nm by used image J software as shown in Fig. 5B.

While transmission electron microscopy results, as indicated in Fig. 6A, show the obtained nanoparticleTiO_2NPs size and distribution that the majority of particle sizes range from 5 to 40 nm, however, it was experiential that increasing the pulsed laser resulted in the production of larger nanoparticle sizes and smaller vacuums. The smaller vacuums obtained with high-pulsed lasers increase the oxidation rate of molecules by letting the direct way of oxygen particles inward from the nearby environment[57]. When the laser pulse interacts with the surface of the target immersed in the D.W., its properties from the plasma generated in the interaction area between the laser pulse and the target surface are affected. The TEM image in Fig. 6B demonstrates the CIP@TiO_2NPs mixture subjected to like conditions as the first step. This resulted in a notable

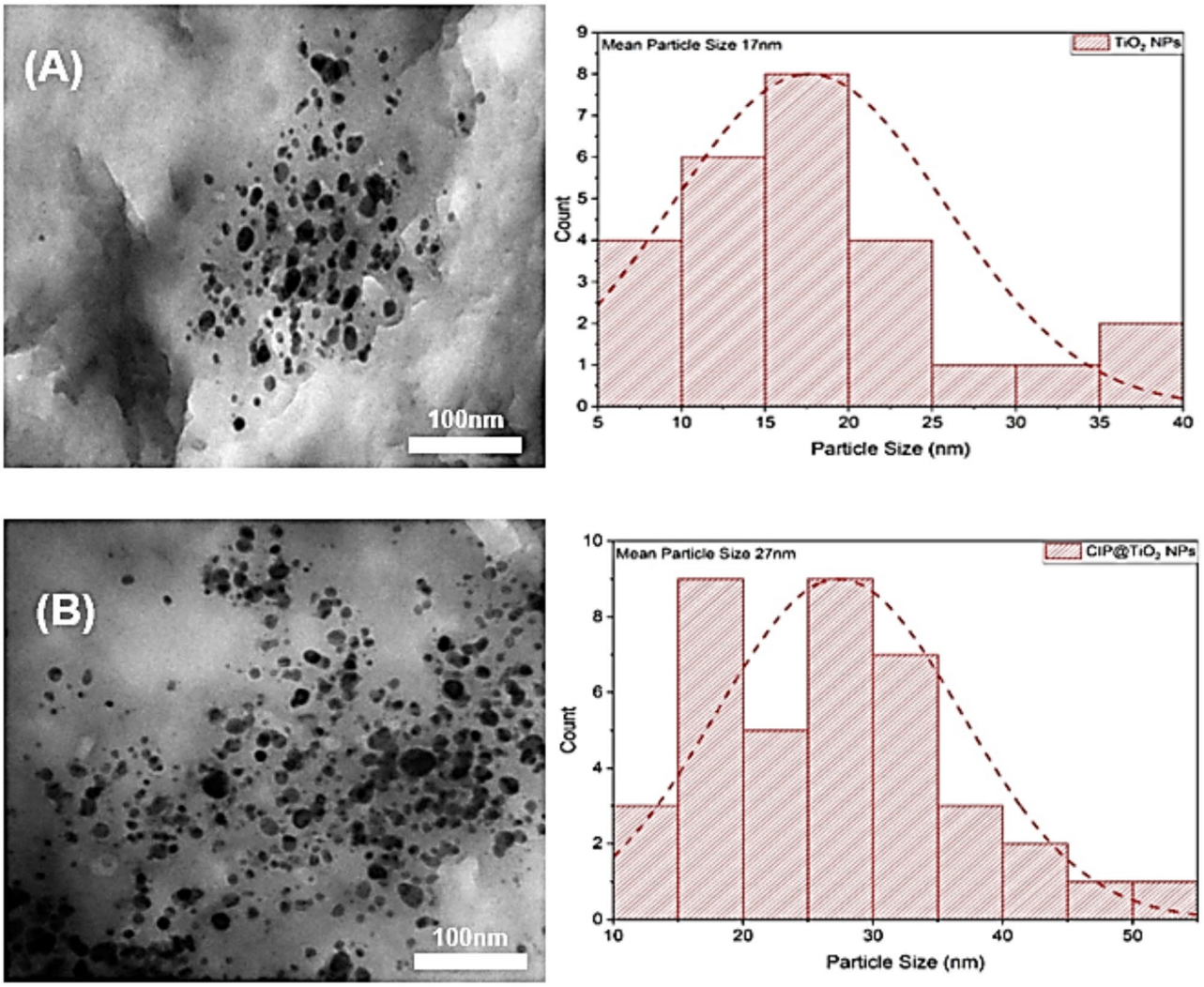

Fig. 6. TEM image for (**A**) TiO_2NPs, (**B**) CIP@TiO_2NPs.

concentration within the plasma and a rapid reduction in temperature. The presentation indicates a size ranging from 5 to 45 nm, with an average diameter of 27 nm, dominated by sphere-shaped nanoparticles. The interaction of the laser pulse with the target surface immersed in distilled water changes its properties, which is essential to plasma generation at the interaction area between the laser pulse and the target exterior.

Further, the biological constructs of the tests, displayed in Fig. 7, were studied utilizing FTIR. The CIP@TiO_2NPs' FTIR assay demonstrated a successful CIP combo that can be both about and private to the NPs. Due to the OH and the symmetry stretch of the N–H bonds, CIP has an essential group at 3253 cm-1. CH2 stretch connects to the 3287 cm-1 region. The C-O vibration in CIP is accountable for the peak height at 1026 cm-1, while the asymmetry C-H bend of the CH_2 group is to blame for the peak centered at 1375 cm-1. Aa stretch (amides I) at NH stretch (amides II) account for the elevations at 1641 and 1026 cm-1. TiO_2NPs' FTIR spectrum presented an extensive absorption band centered at 710 cm-1 in the 500–800 cm-1 spectrum, corresponding with Ti–O–Ti stretch vibrations. This indicates that TiO_2NTs were successfully created. The band that appeared at 3437 cm-1 correlates to the groups of OH that were generated from the electrolyte particles throughout the anodizing procedure and were observed on the outermost layer of the TiO_2NPs assay. The Ti–OH phase and the absorbed H_2O winding mode can be followed at 1641 cm-1. Ti–O modes formed a band at 2159 cm-1. The hydroxyl groups that are part of the water absorbed on the outer layers of the TiO_2NPs are to blame for the bands that appear at 3500 and 3000 cm-1.

Molecular Docking simulation

Data processing and prediction

Fifty conformational structures will be examined based on binding energy (B.E) and other energetic parameters involving electrostatic (vdW), hydrogen bond (HB), and de-solvation energies. The 8JGW protein target was ready to be used as the designed ligand's receptor input. Table 1 presents the conformational structures that

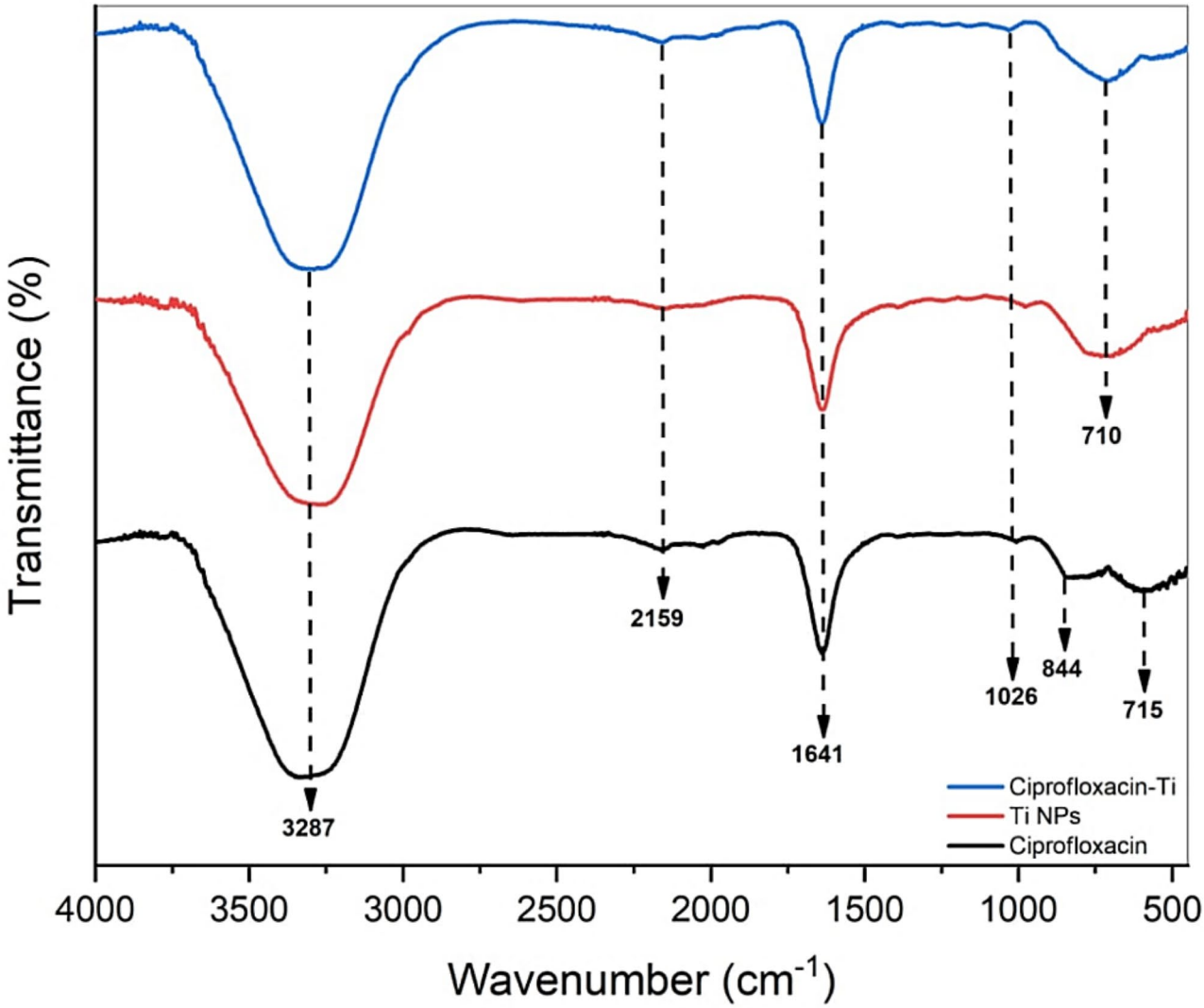

Fig. 7. FTIR of CIP, TiO_2NPs, and CIP@TiO_2NPs.

explore the most significant analyzable energies that primarily contribute to the stability of the ligand-target relationship[5].

Conformational Docking analysis

In docking analysis, the ideal search is for close contacts and non-covalent interactions between the ligand atoms and the target protein's amino acids. The best of 50 produced conformers was exported after the intended ligand was docked against two selected *K. pneumoniae* and *S. mutans* enzymes, as illustrated in Figs. 8 and 9. Based on the role and function of amino acids contained in proteins, analysis of the two docking rounds reveals variations in the position of the ciprofloxacin@TiO_2 adsorption system.

For the best-docked pose analyzed through *K. pneumoniae* ID: 8JGW, the predicted binding energy value of -9.61 kcal/mol indicates a considerable inhibitory behavior in the study. Several non-covalent interactions favored improving the binding affinity of the complex. In such interactions, conventional hydrogen bonds are shaped among the oxygen of Ciprofloxacin and the amino acids of HIS 384 and ARG 410. Other favorable carbon-hydrogen bonds are present between the oxygen of TiO_2NPs and HIS 384. Several ligand-NPs interactions, such as metal-acceptor, π-π stacked, and π-alkyl interactions, are present with HIS 384 and TYR 387. Van der Waals forces were found with ASN 377, ILE 376, and ARG 383[58]. In the case of *S. mutans* ID: 3IHK, the anticipated binding energy value of -9.40 kcal/mol shows a significant inhibitory behavior in the investigation. Several non-covalent interactions supported raising the complex's binding affinity. Conventional hydrogen bonds are created in these interactions between the amino acids of LEU 206 and the oxygen of TiO_2 NPs. Additional advantageous carbon-hydrogen bonds exist between ILE 204 and the Ciprofloxacin adsorbed molecule. There are several ligand-TiO_2 interactions with PHE 98, ILE 181, and ILE 204, including π-π T-formed, alkyl, and π-alkyl connections. It was discovered that PHE 110, LEU 126, ASN 131, PHE 135, SER 153, SER 183, VAL 202, and THR 206 have van der Waals forces. However, unfavorable interaction in this docked pose may stabilize

Conformer No.	CIP@TiO_2 NPs with 8JGW		CIP@TiO_2 NPs with 3IHK	
	Binding energy (Kcal/mol)	vdW, HB, and de-solvation energies	Binding energy (Kcal/mol)	vdW, HB, and de-solvation energies
1	− 9.61	− 11.7	− 9.40	− 11.49
2	− 8.99	− 11.08	− 8.99	− 11.08
3	− 8.2	− 10.28	− 8.85	− 10.94
4	− 7.79	− 9.87	− 7.73	− 9.82
5	− 7.73	− 9.82	− 7.71	− 9.80
6	− 7.73	− 9.82	− 7.48	− 9.57
7	− 7.71	− 9.8	− 7.34	− 9.42
8	− 7.65	− 9.74	− 7.28	− 9.37
9	− 7.64	− 9.73	− 7.04	− 9.13
10	− 7.62	− 9.71	− 6.97	− 9.05
11	− 7.56	− 9.65	− 6.94	− 9.02
12	− 7.53	− 9.61	− 6.72	− 8.81
13	− 7.52	− 9.61	− 6.69	− 8.78
14	− 7.5	− 9.59	− 6.65	− 8.74
15	− 7.49	− 9.58	− 6.36	− 8.44
16	− 7.45	− 9.54	− 6.21	− 8.3
17	− 7.42	− 9.51	− 6.16	− 8.25
18	− 7.39	− 9.48	− 5.73	− 7.82
19	− 7.39	− 9.48	− 5.59	− 7.68
20	− 7.32	− 9.41	− 5.32	− 7.4
21	− 7.25	− 9.34	− 4.5	− 6.59
22	− 7.21	− 9.3	− 4.23	− 6.32
23	− 7.15	− 9.24	− 3.64	− 5.73
24	− 6.89	− 8.98	− 3.56	− 5.65
25	− 6.83	− 8.92	− 3.53	− 5.62
26	− 6.83	− 8.91	− 3.5	− 5.59
27	− 6.78	− 8.87	− 2.77	− 4.86
28	− 6.7	− 8.79	− 1.47	− 3.56
29	− 6.63	− 8.71	− 1.44	− 3.53
30	− 6.53	− 8.62	5.13	3.04
31	− 6.33	− 8.42	6.41	4.32
32	− 6.33	− 8.42	10.72	8.63
33	− 6.3	− 8.38	11.11	9.02
34	− 6.28	− 8.37	12.92	10.83
35	− 6.25	− 8.34	18.3	16.21
36	− 6.25	− 8.34	28.75	26.66
37	− 6.25	− 8.33	33.34	31.25
38	− 6.24	− 8.32	37.62	35.53
39	− 6.23	− 8.32	42.04	39.96
40	− 6.19	− 8.28	42.79	40.7
41	− 6.14	− 8.23	53.13	51.05
42	− 6.14	− 8.23	65.03	62.94
43	− 6.09	− 8.18	65.33	63.25
44	− 6.01	− 8.1	82.54	80.46
45	− 5.97	− 8.06	88.42	86.33
46	− 5.96	− 8.05	116.65	114.56
47	− 5.95	− 8.04	128.7	126.61
48	− 5.92	− 8.01	171.64	169.56
49	− 5.63	− 7.72	193.13	191.04
50	− 5.62	− 7.71	279.98	277.89

Table 1. CIP@TiO2 NPs' molecular Docking experiments with K. pneumoniae (ID: 8JGW) and S. mutans (ID: 3IHK) showed 50 conformations.

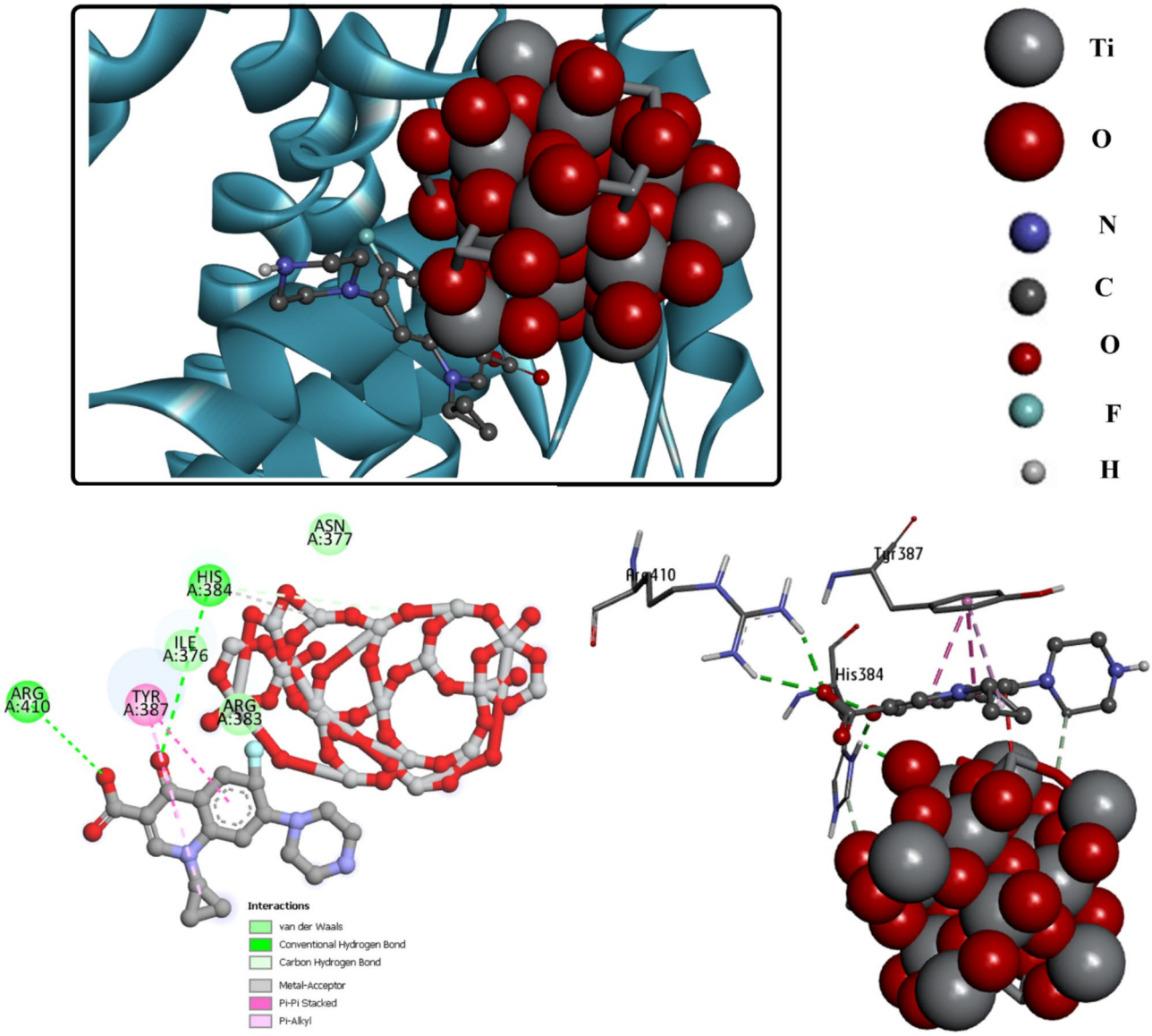

Fig. 8. The greatest posture, 3D, and 2D interactions among CIP@TiO_2 NPs and *K. pneumoniae* (ID: 8JGW).

the complex. Consequently, CIP@TiO_2 NPs complexed with *the K. pneumoniae target have a* higher binding affinity[59].

Assessment of MIC

The study evaluated the effects of CIP, TiO_2NPs, and CIP@TiO_2NPs on the development of *S. mutans* and *K. pneumoniae* bacteria in liquid culture media using turbidity analyses. MICs of < 128–256 µgmL–1 and ≤ 64–128 µgmL–1 for *S. mutans* and *K. pneumoniae*, respectively, are higher for CIP@TiO2NPs than for CIP and TiO_2NPs, according to the current investigation. However, CIP@TiO_2NPs' MICs (≤ 16–32 µgmL–1) against *S. mutans* and *K. pneumoniae* were lower., as shown in Table 2.

Antibacterial activity of CIP@TiO2NPs

As represented in Fig. 10, when CIP was treated alone, the inhibitory zone for the *K. pneumoniae* isolate was chronicled at 18.50 ± 0.12 mm. This inhibitory zone increased to 19.50 ± 0.20 mm when treating TiO_2NPs alone and to 28.50 ± 0.20 mm when CIP was combined with TiO_2NPs (CIP@TiO_2NPs). For *S. mutans*, the inhibitory zone was measured at 14.53 ± 0.20 mm for CIP alone, 8.50 ± 0.01 mm for Tio_2NPs alone, and 17.50 ± 0.10 mm for CIP@TiO_2NPs (as shown in Fig. 11). These experimental circumstances significantly impacted the integrity of bacterial cell walls, resulting in cell lysis, in contrast to the control, which had a zone of inhibition of 6.1 ± 0.10 mm. It is well known that the combination action of TiO2NPs and CIP disrupts the functions of DNA gyrase and the IV enzyme, preventing cell division and ultimately leading to bacterial cell death. Combining nanoparticles (NPs) with antibiotics lowers the dosage required and lowers the possibility of toxicity and the emergence of bacterial resistance. The antibacterial properties of TiO2NPs against every tested isolate are

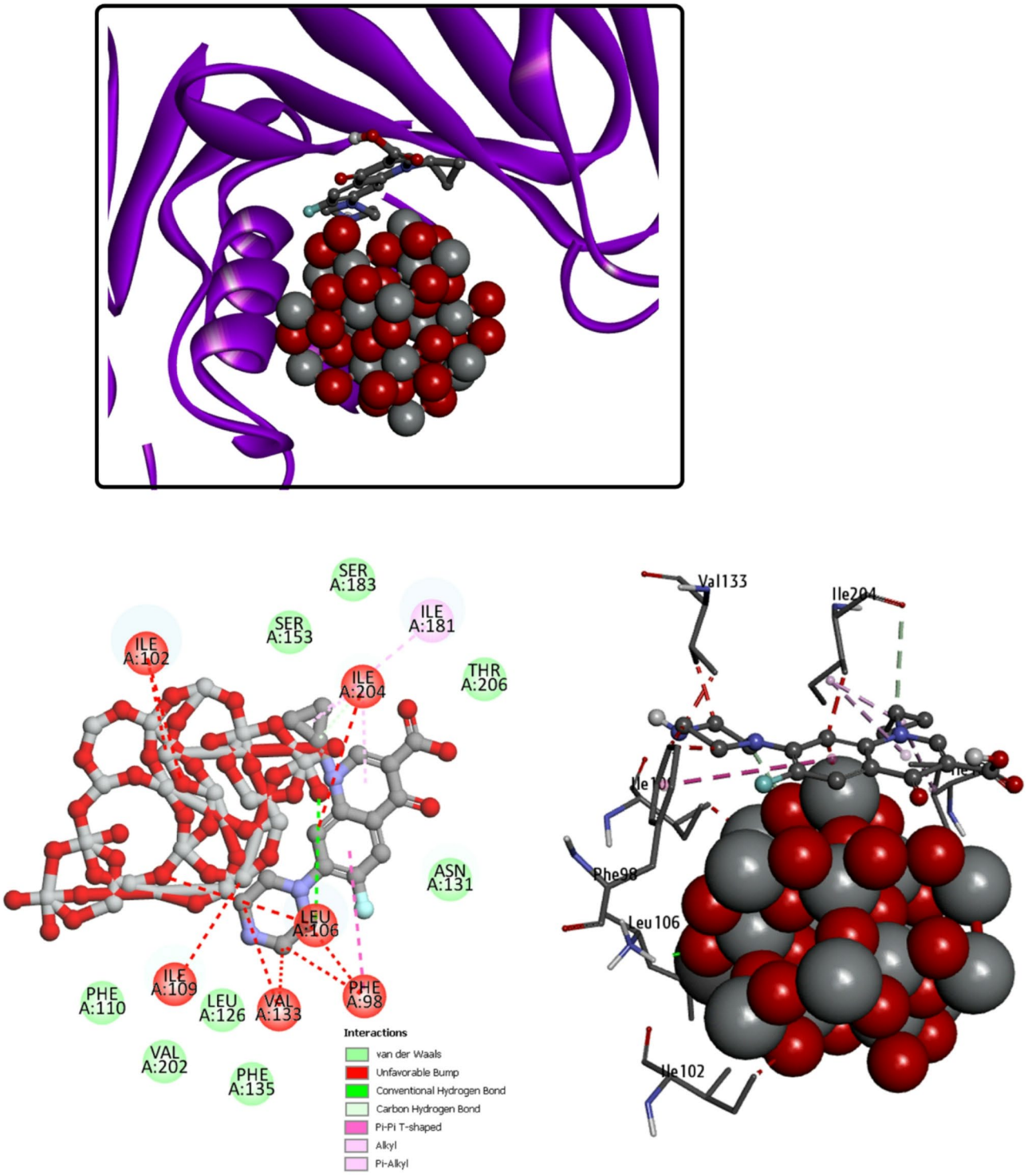

Fig. 9. The greatest posture, 3D, and 2D interactions between CIP@TiO_2 NPs and *S. mutans* (ID: 3IHK).

Isolations	MIC (μgmL^{-1})		
	CIP	TiO_2NPs	CIP@TiO_2NPs
S. mutans	≤ 128	≤ 64–128	≤ 16–32
K. pneumoniae	≤ 256	≤ 128	≤ 32

Table 2. MIC of CIP, TiO_2NPs, CIP@TiO_2NPs.

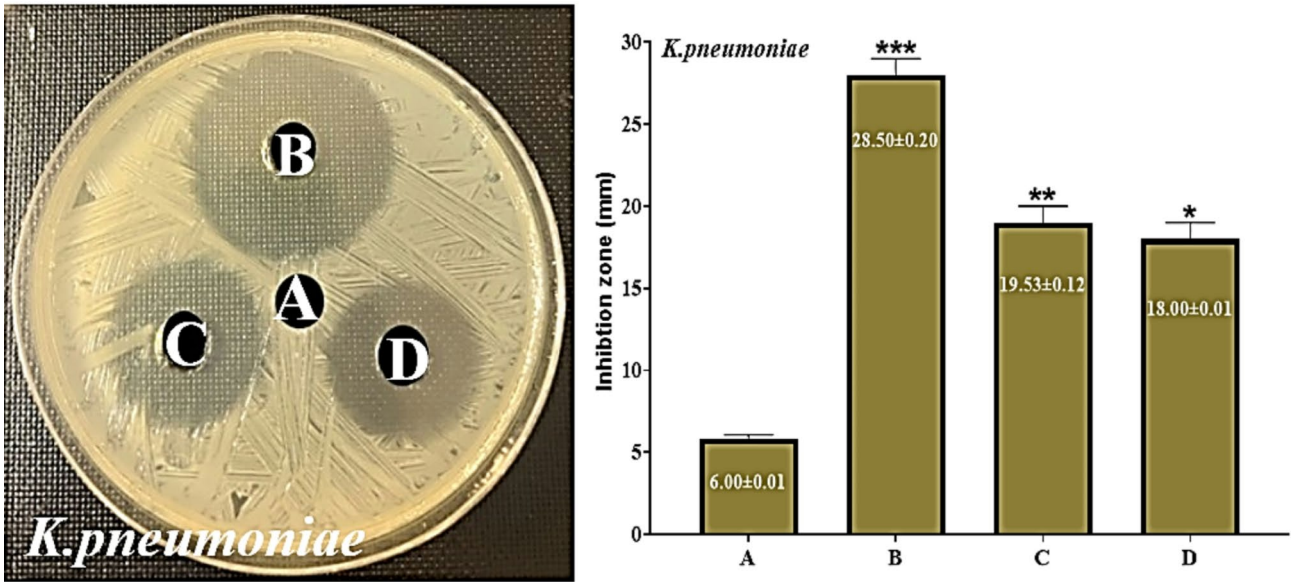

Fig. 10. Synergistic result of CIP@TiO_2NPs against *K. pneumonia.* (**A**) (DW as a negative control. (**B**) CIP@TiO_2NPs treated bacteria. (**C**) CIP treated bacteria. (**D**) TiO_2NPs treated bacteria. $^{*}P \leq 0.05$, $^{**}P \leq 0.01$, $^{***}P \leq 0.001$.

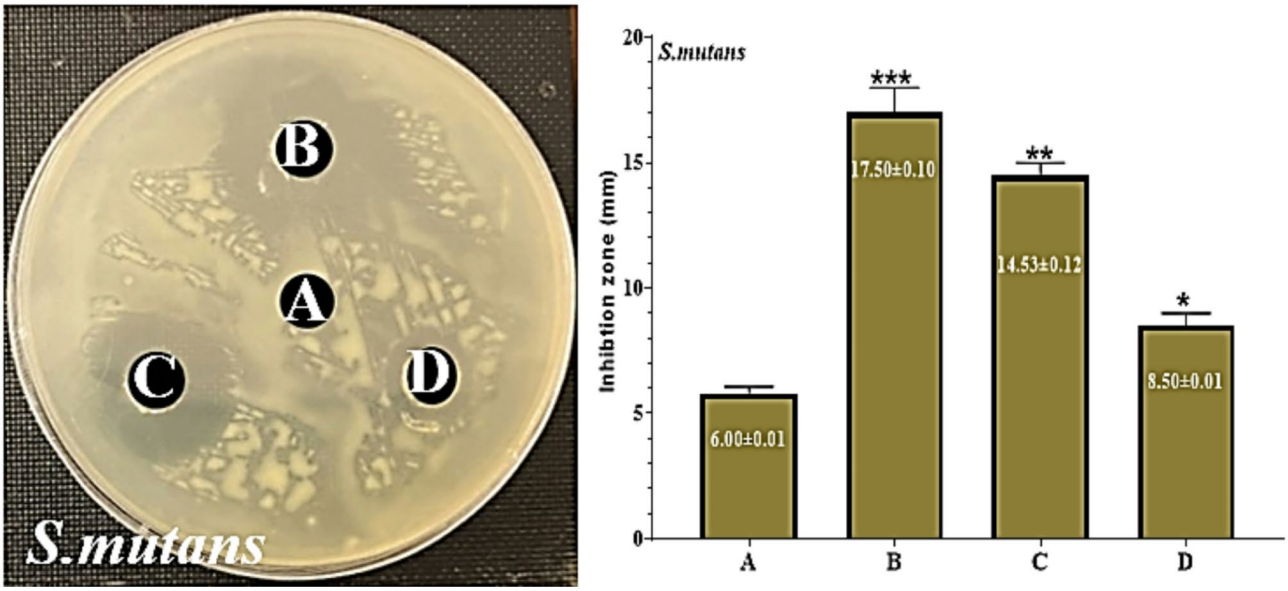

Fig. 11. Synergistic result of CIP@TiO_2NPs against *S. mutans.* (**A**) DW as a negative control. (**B**) CIP@TiO_2NPs treated bacteria. (**C**) CIP treated bacteria. (**D**) TiO_2NPs treated bacteria. $^{*}P \leq 0.05$, $^{**}P \leq 0.01$, $^{***}P \leq 0.001$.

displayed in Figs. 9 and 10. Given that titanium is a metal nanomaterial, this comment highlights how effective it is at treating bacterial adulterations.Also, TiO_2NPs exhibit bio-compatibility and lack cytotoxic properties, making them suitable for addition into various industrial and biomedical applications. The research presented a single-step mixture way for CIP@TiO_2NPs, which established extraordinary synergy in contrast to both types of Gram stain bacteria. Including hydrophilic glycoproteins in conjunction with an interaction of CIP@TiO_2NPs and the cell wall of G + ve bacteria destroys the walls. The damage makes it easier for CIP@TiO_2NPs to penetrate Gram-positive bacteria. Additionally, TiO_2 leakage from the nanoparticles increased membrane permeability in G + ve bacteria, further aiding the entry of CIP@TiO_2NPs. The act of CIP@TiO_2NPs convinced the formation of ROS and phospholipid peroxidation, ultimately creating the demise of bacterial cells[60,61]. The fluorescence microscopy technique was used to study the activity of CIP@TiO_2NPs in killing bacterial strains AO/EtBr double stain. AO/EtBr staining was used in this experiment to identify living from dead bacterial strains. A fluorescent

green light appears when AO binds to the nucleic acid of living bacteria. The adsorption of ethidium bromide on the nucleic acid of dead microbes causes a red or orange colour, as shown in Fig. 12. The live bacterial strains look green, whereas dead ones appear red .

Anti-biofilm activity of CIP@TiO_2NPs

In the current study, we have assessed the anti-biofilm effect of TiO_2NPs, CIP, and CIP@TiO_2NPs against the bacterium *K.pneumoniae* and S. S.mutans strains, which is a important aim for disease. The stain assessment used 0.1% C.V.satin confirmed the existence of bio-films in the tested bacteria. CIP@TiO_2NPs demonstrated significant antibiofilm activity against *S.mutans* compared to *K.pneumoniae*, with a MIC value of 25 μgml^{-1}. The biofilm inhibition of S.mutans was also evaluated through a battery of tests, including microscopic observation, C.V. examination, and EPS secretion by MIC value of 25 μgml^{-1} of TiO_2NPs, CIP, and CIP@TiO_2 NPs. The findings indicated that, in comparison to K. pneumoniae, the MIC dosages of TiO2NPs, CIP, and CIP@TiO2 NPs exhibited a strong anti-biofilm activity against S. mutans, with the highest biofilm reduction occurring at 25 µgml-1. The effects of materials combined with CIP@TiO2 NPs and their capacity to prevent biofilm development are determined by the study's findings. Figure 13 shows the compulsory use of the C.V. stain on the supporter in *K. pneumoniae* and *S. mutans* strains. The C.V. attested to the effectiveness of these formulations in inhibiting the development of biofilms. The results demonstrate that CIP@TiO2 NPs may be regarded as a possible agent for the microbial biofilm reserve. When strains treated with the nanocomposite were compared, it was found that there was less combination and less thick biofilm formation. The K. pneumoniae and S. mutans bacteria treated with the nanocomposite had less aggregation and less dense biofilm formation than the untreated control strains, which exhibited aggregation and were covered in well-developed biofilm structures. These outcomes are consistent with what has been documented in the literature[62].

Conclusions

In cureent study, we successfully created titanium dioxide nanoparticles (TiO_2NPs) conjugated with ciprofloxacin (CIP) and evaluated their antibacterial and anti-biofilm formation activities. SEM consequences exposed nano-spherical almost 40 to 60 nm. CIP @TiO_2 was established after the XRD results with protuberant peaks in (101) and (110) planes. TEM images showed accumulations of sphere-shaped particles. FTIR studies exposed the chemical vibrational promises current. Conferring to the consequences in the current study, the new NPs, CIP@TiO_2NPs, displayed the highest antibacterial and anti-biofilm formation against *K.pneumoniae* and *S.mutans* compared to CIP and TiO_2NPs alone. The molecular docking study revealed strong binding interactions between CIP@TiO_2NPs and *Klebsiella pneumoniae* (ID: 8JGW), with the highest binding energy of -9.61 kcal/mol. These findings suggest that ciprofloxacin-TiO_2 NPs could be effective antibacterial agents against *K. pneumoniae*, potentially enhancing treatment efficacy. Looking ahead, further research could explore the optimization of TiO_2NPs synthesis methods to enhance their stability and effectiveness. Investigating the mechanisms underlying the interaction between TiO_2NPs and various bacterial strains may provide deeper insights into their antibacterial properties. Additionally, the integration of TiO_2NPs with other therapeutic agents could lead to synergistic effects, enhancing their application in clinical settings. Finally, long-term studies assessing the biocompatibility and environmental impact of TiO_2NPs will be crucial to ensure their safe use in medicine. It is crucial to conduct in vivo experiments to assess the therapeutic efficacy and safety of CIP@

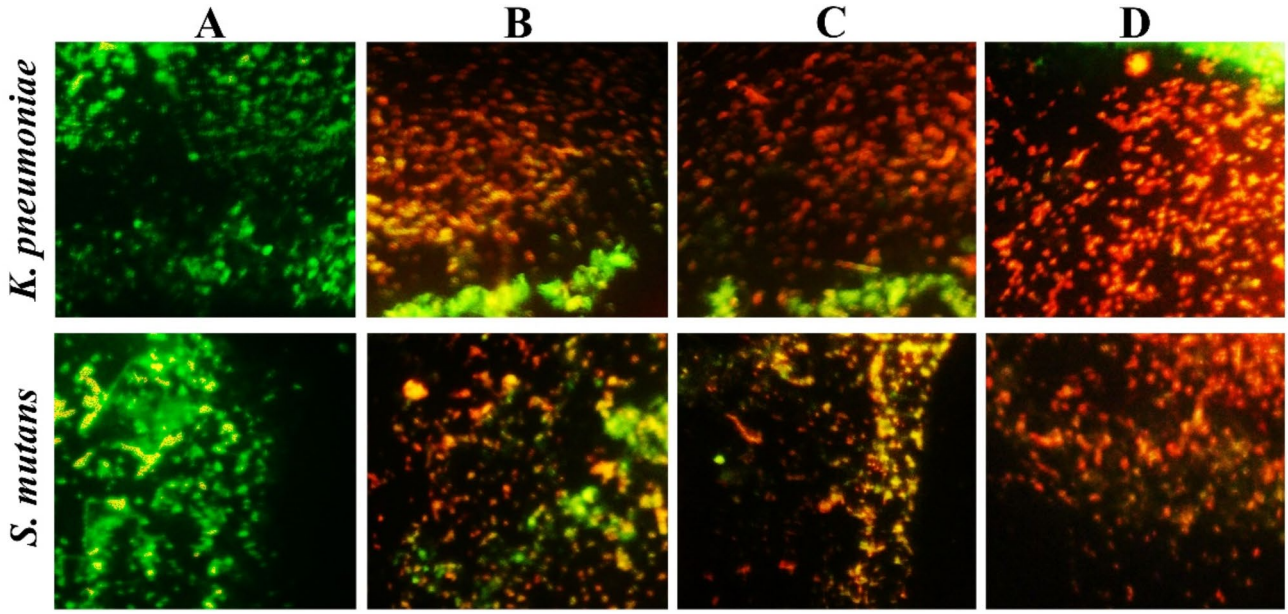

Fig. 12. Live and die bacterial strains after being treated as indicated. (**A**) DW as a negative control. (**B**) Bacteria treated with TiO_2NPs. (**C**) Bacteria treated with CIP. (**D**) Bacteria treated with CIP@TiO_2NPs.

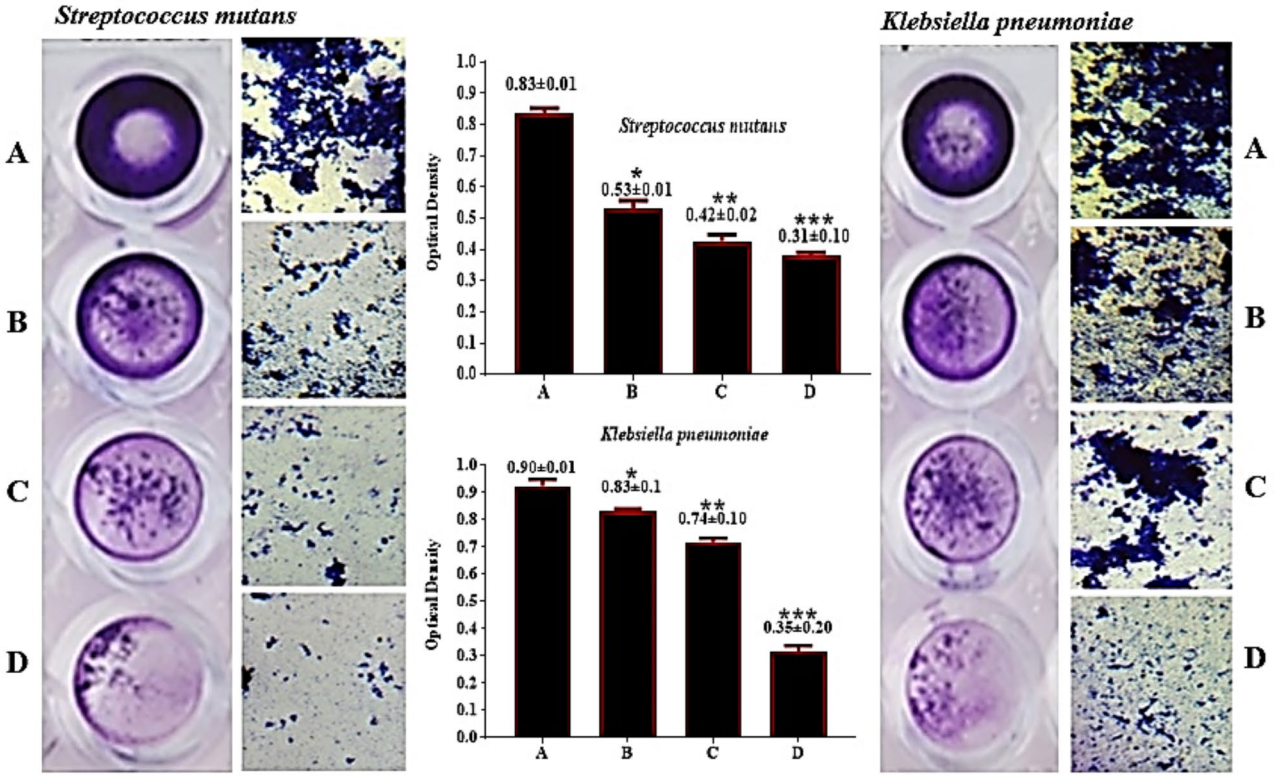

Fig. 13. CIP@TiO_2NPs prevent the formation of bacterial biofilms. (**A**) control untreated bacteria. (**B**) microorganisms were treated with CIP. (**C**) bacteria were treated with TiO_2NPs. (**D**) bacteria treated with CIP@TiO_2NPs. $P \leq 0.05$, ** ≤0.01, and *** ≤0.001.

TiO_2NPs in living organisms. These studies will provide insights into pharmacokinetics, biodistribution, and the biological effects of these nanoparticles in a complex biological environment.This addition aims to provide a forward-looking view that emphasizes the relevance and applicability of our findings in the broader context of biomedical research.

Data availability

Data Availability: Molecular docking and molecular dynamic simulation study using the program m (https://www.chemcomp.com/en/Products.htm).The protein structure used in the present study, obtained from the PDB (Protein Data Bank), is available at (https://www.rcsb.org/structure/7ZWA).

Received: 25 December 2024; Accepted: 7 March 2025
Published online: 23 May 2025

References

1. Khursheed, R., Dua, K., Vishwas, S., Gulati, M., Jha, N. K., Aldhafeeri, G. M., et al. (2022). Biomedical applications of metallic nanoparticles in cancer: current status and future perspectives. Biomedicine & Pharmacotherapy, *150*, 112951.
2. Mordini, D., Mavridi-Printezi, A., Menichetti, A., Cantelli, A., Li, X., & Montalti, M. (2023). Luminescent gold nanoclusters for bioimaging: increasing the ligand complexity. Nanomaterials, *13*(4), 648.
3. Shojaei, S., Shahgholi, M., & Karimipour, A. (2023). The effects of atomic percentage and size of zinc nanoparticles, and atomic porosity on thermal and mechanical properties of reinforced calcium phosphate cement by molecular dynamics simulation. Journal of the Mechanical Behavior of Biomedical Materials, *141*, 105785.
4. Battistelli, G., Proetto, M., Mavridi-Printezi, A., Calvaresi, M., Danielli, A., Constantini, P. E., et al. (2022). Local detection of pH-induced disaggregation of biocompatible micelles by fluorescence switch ON. Chemical Science, *13*(17), 4884–4892.
5. Mavridi-Printezi, A., Guernelli, M., Menichetti, A., & Montalti, M. (2020). Bio-applications of multifunctional melanin nanoparticles: from nanomedicine to nanocosmetics. Nanomaterials, *10*(11), 2276.
6. Saqib, Saddam, Amna Nazeer, Muhammad Ali, Wajid Zaman, Muhammad Younas, Asim Shahzad, Sunera, and Momina Nisar. "Catalytic potential of endophytes facilitates synthesis of biometallic zinc oxide nanoparticles for agricultural application." *BioMetals* 35, no. 5 (2022): 967–985
7. Saqib, Saddam, Wajid Zaman, Asma Ayaz, Sadaf Habib, Saraj Bahadur, Sajjad Hussain, Shabbir Muhammad, and Fazal Ullah. "Postharvest disease Inhibition in fruit by synthesis and characterization of Chitosan iron oxide nanoparticles." Biocatalysis and Agricultural Biotechnology 28 (2020): 101729.
8. Azam, Zara, Asma Ayaz, Muhammad Younas, Zeeshan Qureshi, Bushra Arshad, Wajid Zaman, Fazal Ullah et al. "Microbial synthesized cadmium oxide nanoparticles induce oxidative stress and protein leakage in bacterial cells." *Microbial pathogenesis* 144 (2020): 104188

9. Saqib, Saddam, Wajid Zaman, Fazal Ullah, Imran Majeed, Asma Ayaz, and Muhammad Farooq Hussain munis. "Organometallic assembling of chitosan-Iron oxide nanoparticles with their antifungal evaluation against rhizopus oryzae." Applied Organometallic Chemistry 33, no. 11 (2019): e5190
10. Khan, Zeeshan, Muhammad Irshad, Muhammad Zakria, Saddam Saqib, and Wajid Zaman. "Evaluating the efficacy of endophytic bacteria in controlling rice sheath blight: In vitro and In vivo studies." Microbial Pathogenesis 197 (2024): 107084.
11. Mavridi-Printezi, A., Menichetti, A., Guernelli, M., & Montalti, M. (2021). The photophysics and photochemistry of Melanin-Like nanomaterials depend on morphology and structure. Chemistry–A European Journal, *27*(66), 16309–16319.
12. Mavridi-Printezi, A., Menichetti, A., Ferrazzano, L., & Montalti, M. (2022). Reversible supramolecular noncovalent self-assembly determines the optical properties and the formation of melanin-like nanoparticles. The Journal of Physical Chemistry Letters, *13*(42), 9829–9833.
13. Mavridi-Printezi, A., Menichetti, A., Mordini, D., Amorati, R., & Montalti, M. (2023). Recent applications of melanin-like nanoparticles as antioxidant agents. Antioxidants, *12*(4), 863.
14. Vimbela, G. V., Ngo, S. M., Fraze, C., Yang, L., & Stout, D. A. (2017). Antibacterial properties and toxicity from metallic nanomaterials. International Journal of Nanomedicine, 3941–3965.
15. Banin, E., Hughes, D., & Kuipers, O. P. (2017). Bacterial pathogens, antibiotics and antibiotic resistance. FEMS Microbiology Reviews, *41*(3), 450–452.
16. Muteeb, G., Rehman, M. T., Shahwan, M., & Aatif, M. (2023). Origin of antibiotics and antibiotic resistance, and their impacts on drug development: A narrative review. Pharmaceuticals, *16*(11), 1615.
17. Durán, N., Durán, M., De Jesus, M. B., Seabra, A. B., Fávaro, W. J., & Nakazato, G. (2016). Silver nanoparticles: A new view on mechanistic aspects on antimicrobial activity. Nanomedicine: Nanotechnology, Biology and Medicine, *12*(3), 789–799.
18. Zhang, F., & Cheng, W. (2022). The mechanism of bacterial resistance and potential bacteriostatic strategies. Antibiotics, *11*(9), 1215.
19. Adibkia, K., Omidi, Y., Siahi, M. R., Javadzadeh, A. R., Barzegar- Jalali, M., Barar, J., Maleki, N., Mohammadi, G., & Nokhodchi, A. (2007). Inhibition of endotoxin-induced uveitis by Methylprednisolone acetate nanosuspension in rabbits. Journal of Ocular Pharmacology and Therapeutics, 23(5), 421–432.
20. Yetisgin, A. A., Cetinel, S., Zuvin, M., Kosar, A., & Kutlu, O. (2020). Therapeutic nanoparticles and their targeted delivery applications. Molecules, *25*(9), 2193.
21. Slavin, Y. N., Asnis, J., Hńfeli, U. O., & Bach, H. (2017). Metal nanoparticles: Understanding the mechanisms behind antibacterial activity. Journal of Nanobiotechnology, *15*, 1–20.
22. Egger, S., Lehmann, R. P., Height, M. J., Loessner, M. J., & Schuppler, M. (2009). Antimicrobial properties of a novel silver-silica nanocomposite material. Applied and Environmental Microbiology, *75*(9), 2973–2976.
23. Leid, J. G., Ditto, A. J., Knapp, A., Shah, P. N., Wright, B. D., Blust, R., et al. (2012). In vitro antimicrobial studies of silver carbene complexes: activity of free and nanoparticle carbene formulations against clinical isolates of pathogenic bacteria. Journal of Antimicrobial Chemotherapy, *67*(1), 138–148.
24. Saleh, B. H., Ibrahim, R. N., Abdul-Wahed, H. E., & Salih, Z. T. (2020). Study the Antibacterial Activity of Green Tea Leaves Camellia sinensis Ethanolic Extract against Different Pathogenic bacteria Isolated from Urinary Tract Infections. Plant Archives, 2
25. Habiba, K., Bracho-Rincon, D. P., Gonzalez-Feliciano, J. A., Villalobos-Santos, J. C., Makarov, V. I., Ortiz, D., et al. (2015). Synergistic antibacterial activity of pegylated silver–graphene quantum Dots nanocomposites. Applied Materials Today, *1*(2), 80–87.
26. Durán, N., Marcato, P. D., Conti, R. D., Alves, O. L., Costa, F., & Brocchi, M. (2010). Potential use of silver nanoparticles on pathogenic bacteria, their toxicity and possible mechanisms of action. Journal of the Brazilian Chemical Society, *21*, 949–959.
27. Kaur, A., Preet, S., Kumar, V., Kumar, R., & Kumar, R. (2019). Synergetic effect of Vancomycin loaded silver nanoparticles for enhanced antibacterial activity. Colloids and Surfaces B: Biointerfaces, 176, 62–69.
28. Kabbara, W. K., Ramadan, W. H., Rahbany, P., & Al-Natour, S. (2015). Evaluation of the appropriate use of commonly prescribed fluoroquinolones and the risk of dysglycemia. Therapeutics and Clinical Risk Management, 639–647.
29. Rezvanian, M., Tan, C. K., & Ng, S. F. (2016). Simvastatin-loaded lyophilized wafers as a potential dressing for chronic wounds. Drug Development and Industrial Pharmacy, *42*(12), 2055–2062.
30. Hasoon, B. A., Jawad, K. H., & Abdulsahib, S. S. (2023). Synthesis of Ciprofloxacin-Conjugated Gold Nanoparticles and their Study Antibacterial Effects on Growth Biofilm Formation Through Nebulizer Mask against Respiratory Infection. Plasmonics, 1–15.
31. Peterson, J.W., Petrasky, L.J., Seymour, M.D., Burkhart, R.S., Schuiling, A.B., 2012. Adsorption and breakdown of penicillin antibiotic in the presence of titanium oxide nanoparticles in water. Chemosphere 87, 911–917.
32. Sharma P, Kumari R, Yadav M, Lal R. Evaluation of TiO_2 nanoparticles physicochemical parameters associated with their antimicrobial applications. Indian J Microbiol. 2022;62(3):338–350. doi: https://doi.org/10.1007/s12088-022-01018-9.
33. Van Wieren, E.M., Seymour, M.D., Peterson, J.D., 2012. Interaction of the fluoroquinolone antibiotic, Ofloxacin, with titanium oxide nanoparticles in water: adsorption and breakdown. Sci. Total Environ. 44, 1–9.
34. Paul, T., Miller, P.L., Strathmann, T.J., 2007. Visible-light-mediated TiO2 photocatalysis of fluoroquinolone antibacterial agents. Environ. Sci. Technol. 41, 4720–4727.
35. Blažeka, D., Car, J., & Krstulović, N. (2022). Concentration quantification of TiO2 nanoparticles synthesized by laser ablation of a Ti target in water. Materials, *15*(9), 3146.
36. Adnan, S., Al-dahan, Z. T., & Ghadhban, E. (2019). Titanium dioxide nanoparticles synthesis by pulsed laser ablation. Int. J. Eng. Sci, *8*, 28–32.
37. Hasoon, B. A., Jawad, K. H., Mohammed, I. S., Hussein, N. N., Al-azawi, K. F., & Jabir, M. S. (2024). Silver nanoparticles conjugated amoxicillin: A promising nano-suspension for overcoming multidrug resistance bacteria and preservation of endotracheal tube. Inorganic Chemistry Communications, *165*, 112456.
38. Kassem, A., Abbas, L., Coutinho, O., Opara, S., Najaf, H., Kasperek, D., et al. (2023). Applications of fourier Transform-Infrared spectroscopy in microbial cell biology and environmental microbiology: advances, challenges, and future perspectives. Frontiers in Microbiology, *14*, 1304081.
39. Liang, C., Jia, Z., & Chen, R. (2023). An automated particle size analysis method for SEM images of powder coating particles. Coatings, *13*(9), 1547.
40. Pyrz, W. D. & Buttrey, D. J. Particle size determination using tem: A discussion of image acquisition and analysis forthe novice microscopist. *Langmuir* **24**, 11350–11360. https://doi.org/10.1021/la801367j. (2008).
41. Zhang, S., & Wang, C. (2023). Precise analysis of nanoparticle size distribution in TEM image. Methods and Protocols, *6*(4), 63.
42. Mazhar, A., Elkholy, N. S., Yousif, N. M., & Shalaby, M. S. (2023). Investigations of structural, optical, thermal, and spectroscopic characteristics of CdO-Ni nanoparticles employed in anti-cancer activities for cancer cells. Results in Chemistry, *6*, 101204.
43. Sheltagh, E. R., Almukhtar, O., Rafeeq, M. F., Rasool, K. H., Mahdi, S. A., Jawad, K. H., et al. (2024). Synthesis, pharmaceutical properties, and in Silico study of ZnO@ TiO2 nanocomposite. Inorganic Chemistry Communications, 169, 112994.
44. Rizvi, S. M. D., Shakil, S., & Haneef, M. (2013). A simple click by click protocol to perform docking: AutoDock 4.2 made easy for non-bioinformaticians. EXCLI Journal, *12*, 831.
45. Yasmin, S., Azam, M. G., Hossain, M. S., Akhtar, U. S., & Kabir, M. H. (2024). Efficient Removal of Ciprofloxacin from Aqueous solution using Zn-C battery derived Graphene oxide enhanced by Hydrogen Bonding, Electrostatic and π-π Interaction. *Heliyon*.

46. Shivanika, C., Kumar, D., Ragunathan, V., Tiwari, P., & Sumitha, A. (2020). Molecular docking, validation, dynamics simulations, and pharmacokinetic prediction of natural compounds against the SARS-CoV-2 main-protease. *Journal of biomolecular structure & dynamics*, 1.
47. Soudani, W., Hadjadj-Aoul, F. Z., Bouachrine, M., & Zaki, H. (2021). Molecular Docking of potential cytotoxic alkylating carmustine derivatives 2-chloroethylnitrososulfamides analogues of 2-chloroethylnitrosoureas. Journal of Biomolecular Structure and Dynamics, *39*(12), 4256–4269.
48. Huseby, D. L., Cao, S., Zamaratski, E., Sooriyaarachchi, S., Ahmad, S., Bergfors, T., et al. (2024). Antibiotic class with potent in vivo activity targeting lipopolysaccharide synthesis in Gram-negative bacteria. *Proceedings of the National Academy of Sciences*, *121*(15), e2317274121.
49. Skinner, J. (2018). Statistics for immunologists. Current Protocols in Immunology, *122*(1), e54.
50. Sameen, A. M., Jabir, M. S., & Al-Ani, M. Q. (2020, March). Therapeutic combination of gold nanoparticles and LPS as cytotoxic and apoptosis inducer in breast cancer cells. In *AIP Conference Proceedings* (Vol. 2213, No. 1). AIP Publishing.
51. Andrade, C. (2020). Understanding the difference between standard deviation and standard error of the mean, and knowing when to use which. Indian Journal of Psychological Medicine, *42*(4), 409–410.
52. Martinez, M. N., & Bartholomew, M. J. (2017). What does it "mean"? A review of interpreting and calculating different types of means and standard deviations. Pharmaceutics, *9*(2), 14.
53. Ullah, Fazal, Saddam Saqib, Wajid Zaman, Wajid Khan, Ling Zhao, Adnan Khan, Wasim Khan, and You-Cai Xiong. "Mitigating drought and heavy metal stress in maize using melatonin and sodium nitroprusside." Plant and Soil (2024): 1–23
54. Ullah, Fazal, Saddam Saqib, Wasim Khan, Ling Zhao, Wajid Khan, Meng-Ying Li, and You-Cai Xiong. "Sodium nitroprusside and melatonin improve physiological vitality and drought acclimation via synergistically enhancing antioxidant response in dryland maize." Journal of Plant Growth Regulation (2024): 1–18.
55. Mondal Roy, S., Sharma, B. K., & Roy, D. R. (2021). Synthesis of Ciprofloxacin drug capped silver nanoparticles and their antimicrobial activity: A joint spectrophotometric and density functional investigation. Journal of Cluster Science, *32*, 1575–1584.
56. Ibraheem, H. H., Issa, A. A., & El-Sayed, D. S. (2024). Structural behavior and surface layer modification of (E)-N'-((1H-indol-3-yl) methylene)-4-chlorobenzohydrazide: spectroscopic, DFT, biomedical activity and molecular dynamic simulation against Candida albicans receptor. Journal of Molecular Structure, *1312*, 138484.
57. Zhang, Y., Chen, Y., Chen, C., Zhu, Y., Liu, M., & Chen, J. (2024). The enhancement mechanisms of mucin and lactoferrin on α-amylase activity in saliva: exploring the interactions using QCM-D and molecular Docking. International Journal of Biological Macromolecules, *257*, 128710.
58. Gopalakrishnan, R., & Raghu, K. (2014). Biosynthesis and characterization of gold and silver nanoparticles using milk Thistle (Silybum marianum) seed extract. Journal of Nanoscience, *2014*(1), 905404.
59. Crystallite, X. R. D. (2022). *Size Calculator (Scherrer Equation)—InstaNANO*.
60. Sodagar, A., Akhoundi, M. S. A., Bahador, A., Jalali, Y. F., Behzadi, Z., Elhaminejad, F., & Mirhashemi, A. H. (2017). Effect of TiO2 nanoparticles incorporation on antibacterial properties and shear bond strength of dental composite used in orthodontics. Dental Press Journal of Orthodontics, *22*(05), 67–74.
61. Ammendolia, M. G., & De Berardis, B. (2022). *Nanoparticle Impact on the Bacterial Adaptation: Focus on Nano-Titania. Nanomaterials 2022, 12, 3616*.
62. Guerra, M. E. S., Destro, G., Vieira, B., Lima, A. S., Ferraz, L. F. C., Hakansson, A. P., et al. (2022). Klebsiella pneumoniae biofilms and their role in disease pathogenesis. Frontiers in Cellular and Infection Microbiology, *12*, 877995.

Acknowledgements

This work was supported by the Researchers Supporting Project number (RSP2025R393), King Saud University, Riyadh, Saudi Arabia.

Author contributions

Conceptualization and methodology; M.A.N., H.A.S, S.T.H, and K.H.J.; formal analysis, B.A.H, M.S.J., and A.A.I; Investigation and data curation S.A., M.K.G., and M.H.M; validation M.K.G., and M.H.M; Visualization, original draft preparation, S.A., and M.S.J.; writing—review and editing, S.A., and B.A.H.; supervision, S.A., M.S.J., and M.K.G.; project administration, M.S.J., and B.A.H. All authors have read and agreed to the published version of the manuscript.

Funding

No funding was obtained for this study.

Declarations

Competing interests

The authors declare no competing interests.

Additional information

Correspondence and requests for materials should be addressed to M.S.J., S.A. or M.K.G.